OPEN

Integrated Analysis Of Immunotherapy Treated Clear Cell Renal Cell Carcinomas: An Exploratory Study

Bettina Sobottka, Ronny Nienhold,† Marta Nowak,* Juergen Hench,‡ Pirmin Haeuptle,§ Angela Frank,† Melanie Sachs,† Abdullah Kahraman,* Holger Moch,* Viktor H. Koelzer,* and Kirsten D. Mertz†‖*

Summary: Molecular or immunological differences between responders and nonresponders to immune checkpoint inhibitors (ICIs) of clear cell renal cell carcinomas (ccRCCs) remain incompletely understood. To address this question, we performed next-generation sequencing, methylation analysis, genome wide copy number analysis, targeted RNA sequencing and T-cell receptor sequencing, and we studied frequencies of tumor-infiltrating $CD8^+$ T cells, presence of tertiary lymphoid structures (TLS) and PD-L1 expression in 8 treatment-naive ccRCC patients subsequently treated with ICI (3 responders, 5 nonresponders). Unexpectedly, we identified decreased frequencies of $CD8^+$ tumor-infiltrating T cells and TLS, and a decreased expression of PD-L1 in ICI responders when compared with nonresponders. However, neither tumor-specific genetic alterations nor gene expression profiles correlated with response to ICI or the observed immune features. Our results underline the challenge to stratify ccRCC patients for immunotherapy based on routinely available pathologic primary tumor material, even with advanced technologies. Our findings emphasize the analysis of pretreated metastatic tissue in line with recent observations describing treatment effects on the tumor microenvironment. In addition, our data call for further investigation of additional parameters in a larger ccRCC cohort to understand the mechanistic implications of the observed differences in tumor-infiltrating $CD8^+$ T cells, TLS, and PD-L1 expression.

Key Words: immune phenotype, renal cell carcinoma, next-generation sequencing, digital pathology, personalized medicine

(*J Immunother* 2022;45:35–42)

Received for publication April 12, 2021; accepted July 15, 2021.

From the *Department of Pathology and Molecular Pathology, University Hospital Zurich, University of Zurich, Zurich; †Institute of Pathology; Departments of §Oncology; ‡Pathology, University Hospital Basel; and ‖University of Basel, Basel, Switzerland.

B.S. and R.N.: shared first authorship.

V.H.K. and K.D.M.: shared last authorship.

K.D.M., B.S., R.N., and V.H.K. conceptualized the study, performed pathology review, reviewed and guided annotation work, performed data analysis and wrote the manuscript. H.M. gave important intellectual input and provided important infrastructure. M.N. performed slide scanning and quality control, annotated scanned images, provided intellectual input, and performed image analysis. A.K. and J.H. performed data analysis of EPIC array results. A.F. and M.S. performed experiments. All authors discussed the included results and contributed to the final manuscript.

Reprints: Bettina Sobottka, Department of Pathology and Molecular Pathology, University Hospital Zurich, Schmelzbergstr 12, Zurich CH-8091, Switzerland (e-mail: annabettina.sobottka-brillout@usz.ch).

Supplemental Digital Content is available for this article. Direct URL citations appear in the printed text and are provided in the HTML and PDF versions of this article on the journal's website, www.immunotherapy-journal.com.

Immune checkpoint inhibition (ICI) has become a new backbone in the treatment of advanced clear cell renal cell carcinoma (ccRCC)[1–3] as reflected in the recent European Association of Urology, European Society for Medical Oncology, and National Comprehensive Cancer Network guidelines.[4] Despite its success, the response to immunotherapy remains clinically unsatisfactory in many RCC patients. The underlying mechanisms are incompletely understood but there is emerging evidence that they may relate to differences within the tumor microenvironment.[5] Recently, single-cell transcriptome analysis revealed the functional effect of treatment on the tumor immune microenvironment of ccRCC.[6] Integrative analysis of tumor intrinsic genetic alterations and RNA expression identified molecular subsets of RCC, and provided important insights into the molecular basis of treatment response to ICI.[7] A broad summary of these molecular subsets was suggested, dichotomizing ccRCC into angiogenic-poorly immunogenic, frequently *PBRM1* mutated, and proliferative-inflamed tumors, the latter commonly carrying loss of function mutations in *BAP1* and/or *CDKN2A*.[8] However, the composition and spatial distribution of the tumor immune infiltrate, the effect of tertiary lymphoid structures (TLS)[9] and their contribution to immune checkpoint inhibitor response remain poorly investigated.

From a clinicopathologic point of view, an improved pretreatment stratification of ccRCC patients for immunotherapy by a combined assessment of tumor-related and microenvironment-associated factors would be desirable. Common predictive biomarkers of immune checkpoint blockade response do not appear to be useful in ccRCC for three reasons: (i) The overall tumor mutational burden in ccRCC is usually low; rare neoantigens predominantly arise from frameshift mutations caused by insertions-deletions (INDELs), splice variants, and post-translational modifications.[10,11] (ii) PD-L1 expression that is usually regarded as a surrogate marker of a pre-existing immune response[12] can be increased in some tumors merely as a consequence of HIF binding to the *PD-L1* promoter.[13,14] (iii) The role of tumor-infiltrating $CD8^+$ T cells, usually associated with a good prognosis in most malignancies,[12] remains controversial mainly because of methodological issues of previous studies such as the failure to control for the different histologic RCC subtypes.[15,16]

To explore potential differences in tumor-related and microenvironment-associated factors of ICI treated ccRCC patients, we performed a multimodal investigation by combining molecular and histologic methods including digital image quantification techniques in a well-defined group of ICI responding (n = 3) and nonresponding (n = 5) ccRCC. For integrated tumor profiling, we combined a suite of analyses: comprehensive targeted parallel sequencing, whole-genome copy number variation (CNV) analysis, targeted transcriptomics and T-cell receptor (TCR) sequencing, spatially resolved digital

immunoprofiling, PD-L1 expression, and histologic assessment of TLS. With the selection of the 2 extremes of the clinical spectrum to ICI response, we hypothesized to uncover biological differences by this integrative in-depth analysis.

MATERIALS AND METHODS

Patient Cohort

Ethical approval was obtained from the Ethics Committee of Northwestern and Central Switzerland (Project-ID 2016-01499). We collected treatment-naive ccRCC cases from the archives of the Institute of Pathology, Cantonal Hospital Baselland, Liestal, Switzerland between 2001 and 2018. Patients showed no synchronous metastases but developed metachronous metastases as indicated. After surgical resection of the primary tumor, the majority of the patients had received first line treatment with tyrosine kinase inhibitors before ICI therapy (anti-PD1, Nivolumab) was initiated upon disease progression, in 1 case in conjunction with anti-CTLA-4 treatment (Ipilimumab). Treatment with ICI varied between 1 and 96 cycles, and ICI response was assessed by imaging (Table 1).

Nucleic Acid Extraction

DNA and RNA was extracted from FFPE tumor and adjacent healthy control tissues using the RecoverAll Total Nucleic Acid Isolation Kit (Catalog No. AM1975; Thermo Fisher Scientific, Waltham, MA). Nucleic acid concentrations were measured with Qubit dsDNA HS and RNA HS Assay Kits (Catalog No. Q32851 and Q32852; Thermo Fisher Scientific).

TABLE 1. Cohort

Retrospective ccRCC Cohort Clinicopathologic Parameters, n = 8	Responder (n = 3), N	Nonresponder (n = 5), N
Age at initial diagnosis		
Age below 60	2	0
Age 60 years or above	1	5
Sex		
Female	2	2
Male	1	3
Tumor (T) stage		
T1	0	1
T2	2	0
T3	0	3
T4	1	1
Fuhrman grade		
Grade 1	1	0
Grade 2	1	2
Grade 3	1	3
Grade 4	0	0
First line treatment		
None	0	2
TKI	3	3
ICI treatment		
Nivolumab	3	4
Nivolumab+Ipilimumab	0	1
ICI cylces		
Average in months	84.7	2.8
Progression free survival		
Average in months	39.3	0

Detailed clinicopathologic information of the study cohort. Only primary tumors from clear cell renal cell carcinoma patients were included and are grouped according to their response to ICI treatment.

ccRCC indicates clear cell renal cell carcinomas; ICI, immune checkpoint inhibitor.

Next-generation Sequencing (NGS)

We performed targeted parallel sequencing of genomic DNA covering hotspot regions of 125 genes using a custom-adapted panel. This panel includes nonoverlapping target regions of the Oncomine Focus Assay, Oncomine Comprehensive Assay v3, Ion AmpliSeq Cancer Hotspot Panel v2, and AmpliSeq Colon and Lung Cancer Research Panel v2 (Supplemental Figs. 1A, B, Supplemental Digital Content 1, http://links.lww.com/JIT/A624). Tumor mutational burden was detected and calculated using the Oncomine Tumor Mutation Load Assay (Catalog No. A37909; Thermo Fisher Scientific) covering the complete coding regions of 409 genes (Supplementary Fig. 1C, Supplemental Digital Content 1, http://links.lww.com/JIT/A624).

Profiling of Immune Response by Targeted RNAseq

We analyzed the differential expression of 398 genes using the Oncomine Immune Response Research Assay (OIRRA, Catalog No. A32881; Thermo Fisher Scientific) as recently described.[17] NGS libraries were prepared according to the manufacturer's description. Demultiplexing and quantification of transcript levels were performed with the standard setting of the ImmuneResponseRNA plugin (version 5.12.0.1) within the Torrent Suite (version 5.12.1), provided as part of the OIRRA. Differential gene expression analysis was performed using the Transcriptome Analysis Console Software (version 4.0.1) from Thermo Fisher Scientific.

Methylation and Copy Number Analysis

A volume of 500 ng genomic DNA from each sample was subjected to bisulfite conversion using the EZ DNA Methylation Kit (Catalog No. D5001; Zymo, Irvine, CA) according to the manufacturer's guidelines. The Infinium Human Methylation EPIC 850 k array was used to obtain genome wide DNA methylation profiles from FFPE tumor samples, according to the manufacturer's instructions (Illumina, USA). Data (IDAT files) were analyzed through the *minfi*[18] R package. Methylation patterns were subjected to unsupervised machine learning on the form of uniform manifold approximation projection (UMAP,[19]), all as previously described.[20] Copy number calculations on the IDAT files were performed using R (version 4.0.4) and the conumee Bioconductor[21] package (version 1.24.0). Before the calculations, IDAT files were imported to R using the *minfi* Bioconductor package (v.1.36.0) and converted to *conumee* compatabile MethylSet objects. Probe sets were downsampled to an Illumina 450K array and intensities were normalized using a reference probe set comprising 33 individuals.[22] Normalized probe intensities were subsequently clustered into segments using the circular binary segmentation algorithm with an acceptance significance level of alpha = 0.05, 10,000 permutations, minimum of 5 probes per segment and without undoing change-points. Copy number spectrum plots were generated using the cnSpec function in the GenVisR[23] Bioconductor package (version 1.22.1).

Immunohistochemistry, Digitalization, and TLS Quantification

Immunohistochemical analysis was performed utilizing the monoclonal mouse-antihuman CD8 (clone 4B11; Leica Biosystems, Muttenz, Switzerland) and the monoclonal rabbit-anti-PD-L1 (clone SP263; Roche Diagnostics, Rotkreuz, Switzerland) antibodies with pretreatments according to the manufacturers' instructions. Antibody binding was visualized using either OptiView (Roche Diagnostics) or Bond Polymer Refine Red Detection (Leica Biosystems) kits. All immunohistochemical stains were part of the diagnostic routine. Stained slides were digitalized on a Hamamatsu NanoZoomer S360 scanner at 40× magnification (Hamamatsu Photonics, Hamamatsu City, Japan). Digital slide review, annotation of tumor regions as recommended by the International Immuno-Oncology Biomarker Working Group[24] and quality controls were performed by an expert image analyst (M.N.) and reviewed by a board-certified pathologist (V.H.K.). A deep neural network (DNN) algorithm (DeepNet, HALO AI on HALO 3.1.1076; Indica Labs, Corrales, NM) was trained using pathologist annotations to automatically localize and measure tumor areas, desmoplastic and inflamed stromal regions in RCC resection specimens and to exclude glass background, areas of tumor necrosis, debris, and tissue folds. Mark-up images for tissue classification were generated, and the accuracy of tissue classification was confirmed by pathologist review. For cell-level analysis, nuclear segmentation was performed using a seeded watershed and optimized using cell-morphometric parameters. Marker-positive cells in stromal and epithelial regions were quantified according to pathologist-set thresholds. $CD8^+$ counts were normalized by area to determine infiltration density in each tumor region and localize it to the stromal or intraepithelial compartment. PD-L1 expression was scored as the combined positive score (percentage of PD-L1 expressing tumor and infiltrating immune cells relative to the total number of tumor cells) by visual assessment of the digital slides.[25] TLS were defined as aggregates of lymphocytes with formation of a lymphoid based on hematoxylin and eosin stain and were counted with frequency/mm^2.[26]

T-Cell Receptor Sequencing

Identification and quantification of unique T-cell clones to determine clonality and diversity of productive T lymphocytes was performed using the Oncomine TCR Beta-SR Assay (Catalog No. A39359; Thermo Fisher Scientific). In brief, 250 ng of RNA extracted from FFPE tumor samples were used to generate first strand cDNA (SuperScript VILO cDNA Synthesis Kit, Catalog No. 11754250; Thermo Fisher Scientific). established gene segments for TCR recombination libraries were generated by amplification of the framework region 3 (FR3, V region), complementarity determining region 3 (CDR3, D region) and joining (J) region and barcoded with the Ion Torrent Dual Barcode Kit 1-96 (Catalog No. A39360; Thermo Fisher Scientific). The libraries were quantified (Ion Library TaqMan Quantitation Kit, Catalog No. 4468802; Thermo Fisher Scientific), equimolarly pooled and sequenced utilizing the Ion GeneStudio S5xl (Thermo Fisher Scientific). Demultiplexing and detection of individual T-cell clones were performed with the standard settings of the Torrent Suite (version 5.12.1) and the Oncomine TCR Beta-SR—w1.0—RNA—Single Sample workflow (version 1.0), provided as part of the Oncomine TCR Beta-SR Assay by Thermo Fisher Scientific.

RESULTS

To identify molecular and morphological differences between ccRCCs of ICI nonresponders and responders we used a multidimensional approach including routine diagnostic, emerging, and exploratory technologies for in-depth investigation of 8 ccRCC patients with differential treatment response (Table 1). Less than half of the patients (n = 3) responded well to ICI therapy as documented by imaging, while the remaining patients showed nonresponse or progressive disease. Comprehensive NGS confirmed the presence of loss of function mutations in the *VHL* gene in 5 of 8 cases, either in isolation or in conjunction with *PBRM1* or *BAP1* alterations (Fig. 1A). One tumor in each group, responders and nonresponders, was *VHL* wild type, carrying genetic variants in *PBRM1* alone or together with *BAP1*, and 1 nonresponder tumor was wild type for *VHL*, *BAP1*, and *PBRM1* (Fig. 1A). All tumors displayed single mutated genes interpreted as passenger mutations (Fig. 1A). The tumor mutational burden was low (< 10 mutations/megabase) for all cases and no increased INDEL frameshifts could be detected (data not shown). For methylation analysis the investigated ccRCC cases were subjected to UMAP against a public reference dataset (n = 18,228), mainly comprising samples from the TCGA, the top 25,000 differentially methylated probes, determined by SD-based ranking. As expected, all analyzed cases (n = 7) grouped within the cluster formed by ccRCC (n = 332) samples (Supplemental Fig. 2, Supplemental Digital Content 2, http://links.lww.com/JIT/A625). However, UMAP analysis did not show separation of these specimens that correlated with their documented immune response state. Most chromosomal aberrations as analyzed by a single-nucleotide polymorphism-based array occurred particularly as chromosome 3p losses and chromosome 5q gains without major differences between responders and nonresponders (Fig. 1B). To analyze markers of ICI response, we assessed tumor-infiltrating $CD8^+$ T cells and PD-L1 expression by immunohistochemistry. As there are yet no established guidelines for $CD8^+$ T-cell assessment in ccRCC, we based our approach on the recently published recommendations of the International Immuno-Oncology Biomarker Working Group.[24] CD8 stained whole slides were scanned at high resolution and quantitatively evaluated by digital image analysis to derive the overall and compartment-specific $CD8^+$ T-cell infiltration densities (ie, specific assessment of the tumor center and the invasive margin; Fig. 2A). We observed poorly (Fig. 2B) and highly (Fig. 2C) $CD8^+$ T-cell-infiltrated tumors. Quantitative analysis revealed an overall (Fig. 2D) and spatial (Fig. 2E) trend toward higher $CD8^+$ tumor-infiltrating T cells in nonresponders across all tumor compartments. Likewise, increased amounts of TLS (Fig. 2F) and PD-L1 expression (Fig. 2G) were detected in nonresponders. Both CD8-infiltration density and PD-L1 expression were independent of the underlying profile of genetic alterations (data not shown). TCR sequencing revealed increased evenness, diversity and TCRβ clones in responders yet with reduced convergence frequencies (Supplemental Fig. 3, Supplemental Digital Content 3, http://links.lww.com/JIT/A626). Of particular interest for the analysis of ICI response biomarkers in ccRCC are transcriptional differences in the tumor microenvironment of $CD8^+$ T-cell-rich but nonresponding ccRCCs in comparison to $CD8^+$ T-cell-poor but responding ccRCC samples. Despite clear differences in the inflammatory milieu between tumor and matched healthy normal samples (Fig. 3A) we could not observe any significant differences in gene expression profiles between

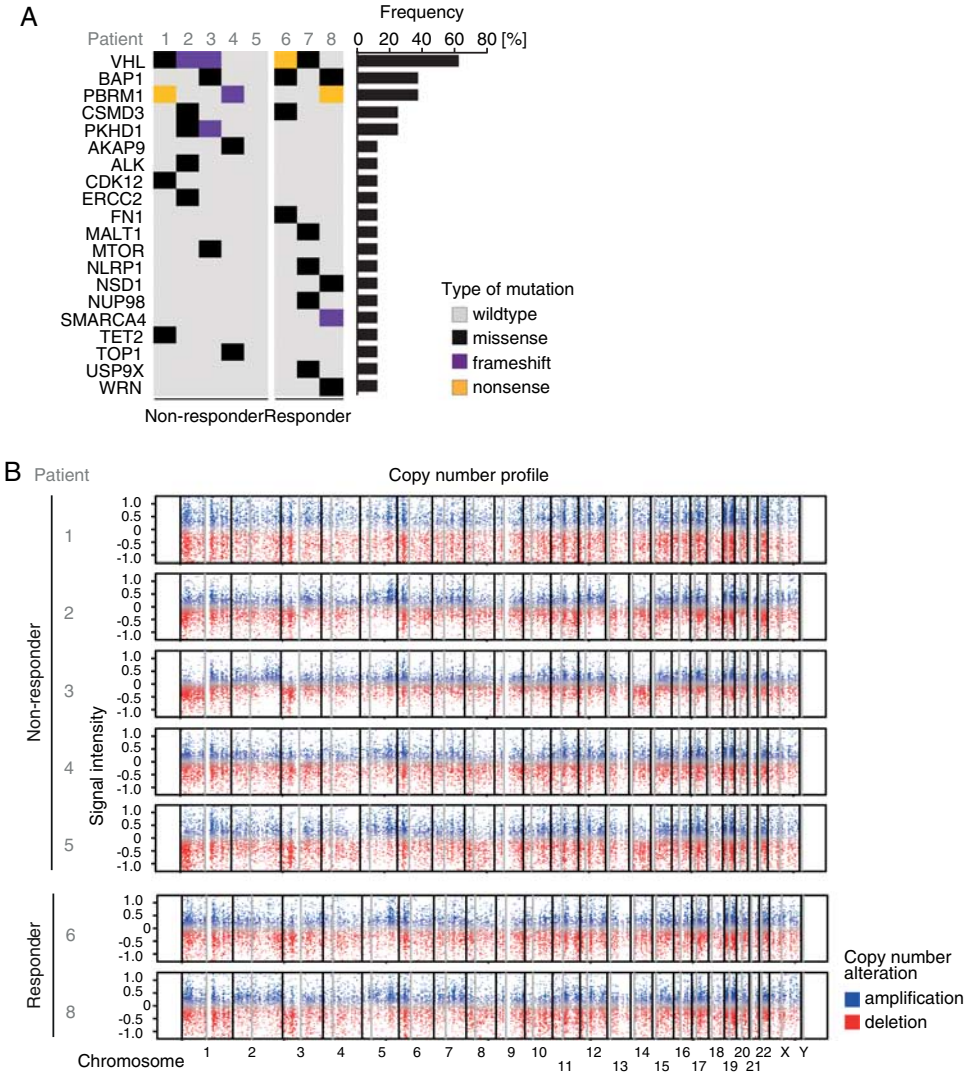

FIGURE 1. Mutational and whole-genome wide copy number variation landscape in responders and nonresponders. Oncoprint visualizes per gene (left) the mutational frequencies (right) for our cohort including the mutation type (grey shading). The majority of clear cell renal cell carcinomas samples showed genetic alterations in *VHL* with or without co-altered genes. *VHL*, *PBRM1*, and *BAP1* were the most frequently co-altered genes. Single mutated genes in nonresponders versus responders displayed no overlapping genetic alterations (A). Whole-genome wide SNP-based copy number variation analysis revealed the expected variations particularly in chromosome 3p with similar distributions between responders and nonresponders (B). SNP indicates single-nucleotide polymorphism.

responding and nonresponding tumors (Fig. 3B). Also, no substantial differences of genetic variant effects and gene expression could be detected with respect to ICI treatment response (Fig. 3B) or alone (Figs. 3C, D).

DISCUSSION

Here we present a multidimensional analysis of treatment-naive ccRCC resection specimens subsequently treated with immune checkpoint inhibitors to uncover cellular, molecular, and histologic differences of ICI responders and nonresponders in ccRCC. We focused on samples that represent the typically available tissue within pathology departments, and combined established methods like NGS and immunohistochemistry with novel technologies with potential for integration in future pathology workflows such as digital quantification of immunohistochemistry, targeted RNA and TCR sequencing.

In contrast to previous reports,[27,28] we did not observe a higher frequency of loss of function variants in *PBRM1* or *BAP1* or a particular immunogenic phenotype in association with treatment response. While whole-exome sequencing or whole-genome sequencing might have elucidated additional genetic alterations between responders and nonresponders, our comprehensive NGS panel covered the known relevant genes in ccRCC[29,30] necessary for the classification of ccRCCs into the 2 large groups associated with an either angiogenic or proinflammatory microenvironment.[8] Methylation analysis reliably grouped the investigated ccRCC samples into the expected ccRCC clusters, yet without distinct features between responders and nonresponders. In our cohort, the tumor mutational burden was low as expected, and consistently, INDEL frameshifts which were proposed as a potential source

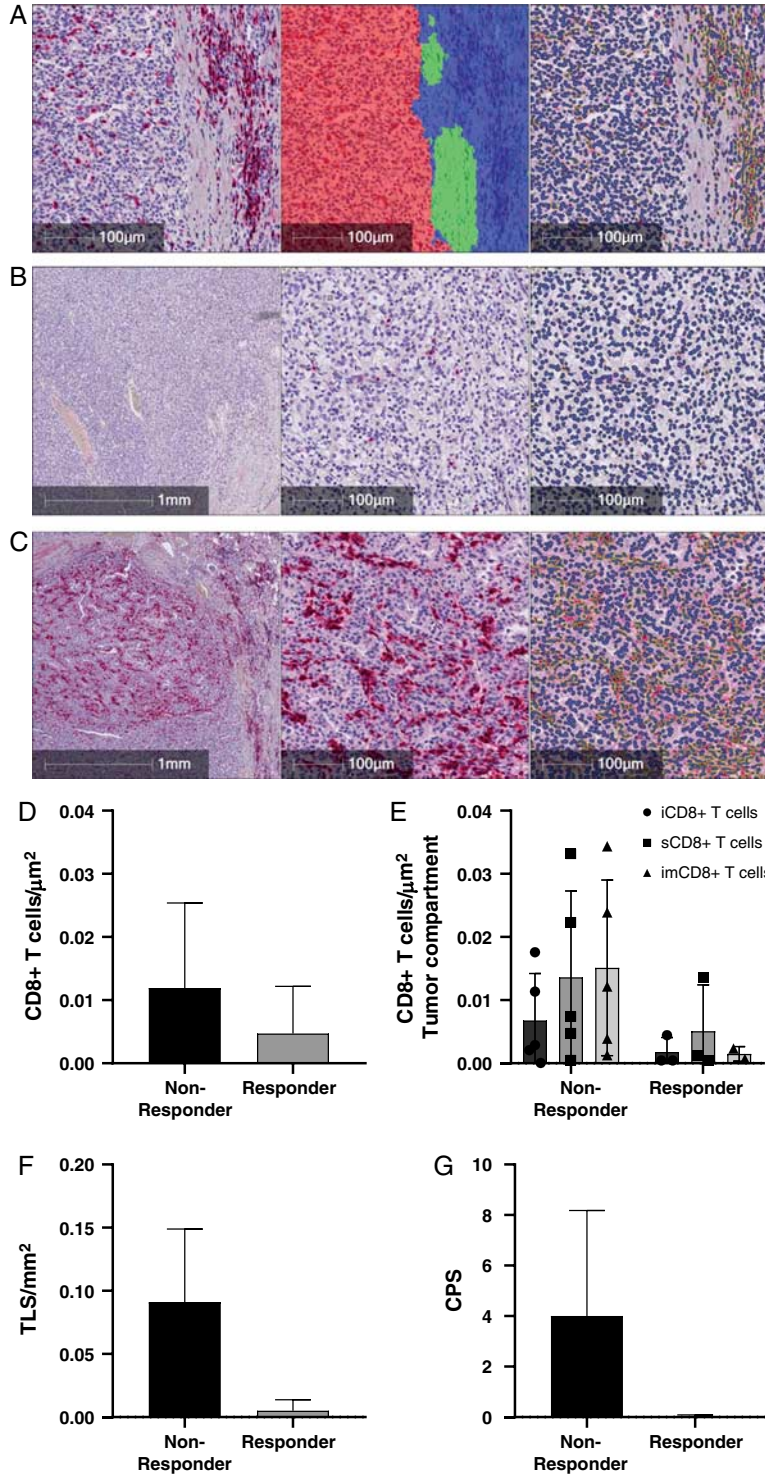

FIGURE 2. CD8⁺ tumor-infiltrating T cells, TLS, and PD-L1 expression in responders versus nonresponders. CD8 stained whole sections were digitalized and annotated according to the state-of-the-art recommendations including the tumor center (red) and the invasive margin (blue) with lymphocyte poor areas (green) (A). The CD8⁺ T-cell infiltrate was sparse (far left and middle B) or dense (far left and middle C) and was analyzed at single-cell resolution including spatial distribution (far right B and C). Absolute (D) and compartment-specific (E) CD8⁺ T-cell densities, as well as the presence of TLS (F) and PD-L1 expression depicted as the combined positivity score (CPS) (G) were increased in nonresponders compared with responders. iCD8⁺ T cells = intratumoral CD8⁺ T cells, sCD8⁺ T cells = stromal CD8⁺ T cells, imCD8⁺ T cells = invasive margin CD8⁺ T cells.

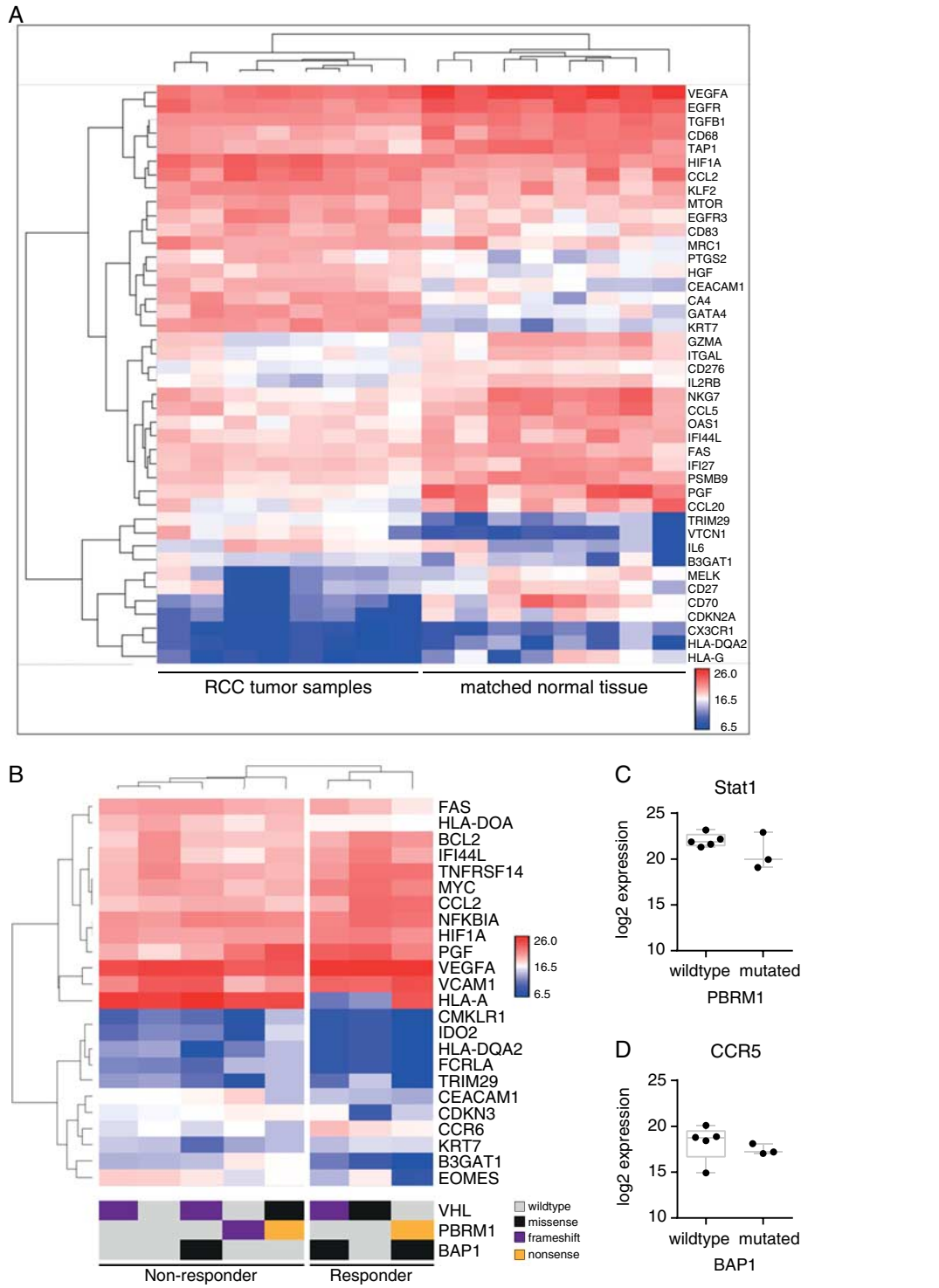

FIGURE 3. Gene expression profiles of the tumor microenvironment. Heat-map of fold change expression of 398 genes between all tumors and matched normal tissue reveals a more inflammatory environment in tumor samples when compared with the healthy matched control tissue (A). Heat-map of top differentially ($P < 0.05$) expressed gene expression profiles of responders and nonresponders, only B3GAT1 also reached a false discovery rate < 0.05 (B). Similar distribution of genetic alterations and variant effects between nonresponders and responders (B, at the bottom) without any appreciable effect on gene expression. In detail, neither genetic alterations in *PBRM1* (C) nor in *BAP1* (D) showed differences in the expression of potential target genes. Heat-maps display log2 expression of each gene normalized to housekeeping genes.

of neoantigenicity in ccRCC[10] were rare without significant differences in responders versus nonresponders (data not shown). As abnormalities in chromosomal structure increase genetic variability and could be another source of mutational burden,[31] we performed whole-genome CNV analysis. Our data reflect the known CNV landscape of RCC[32,33] that has recently been expanded by a comprehensive TCGA analysis revealing characteristic gains and losses particularly within chromosome 3p and 5q[29] with only few studies available in the clinical context and with regard to metastatic disease.[34]

Unexpectedly we identified increased $CD8^+$ tumor-infiltrating T cells, TLS, and PD-L1 expression in ICI nonresponders when compared with responders. Unlike most studies, we present a spatially resolved, highly standardized, and reproducible assessment of tumor-infiltrating $CD8^+$ T cells by employing digital image analysis according to the state-of-the-art guidelines for tumor infiltrating lymphocytes assessment.[24,35] As standardized PD-L1 assessment algorithms in ccRCC are not available, we reported our findings as the combined positivity score.[25] All 3 parameters are generally regarded as indicators of a successful pretreatment immune response.[9,12] Our observations associating elevated $CD8^+$ T-cell frequencies with poor treatment response are particularly counterintuitive, because $CD8^+$ T cells represent the major target population of anti-PD1 treatment.[36] Very recent findings[6] suggest that both the tumor and the tumor immune microenvironment are shaped by the respective treatment performed after excision of the primary tumor. These observations may explain the observed discrepancy between tissue level features and outcome considering the time interval between resection and immune oncology treatment in the present study. Likewise, in light of this recent publication[6] our data strongly support the evaluation of progressing tumor lesions as the original primary tumor may not reflect the immune cell composition that is indicative of immunotherapy response. In line with prior reports, the predictive and prognostic role of tumor-infiltrating $CD8^+$ T cells in ccRCC therefore continues to be controversial.[15,16,37–39] Some studies have found high $CD8^+$ T cells in ccRCCs of poor ICI responders.[15,39] Conflicting findings about the predictive value of $CD8^+$ T-cell frequencies may result from (i) the lack of standardized and quantitative tumor-infiltrating immune cell assessment algorithms, (ii) investigation of different tumor compartments, (iii) heterogeneous assessment of additional markers relating to immune phenotypes, (iv) lack of spatial information and (v)—maybe most importantly—no clear separation of the different histologic RCC entities within investigated cohorts, leading to a mixture of different histologic subtypes in these previous investigations with associated differences in the tumor microenvironment[15,16] Moreover, the application of PD-L1 as a biomarker in ccRCC[25] remains controversial as it can be increased upon persistent HIF expression or hypoxia.[13,14,40]

To elucidate potential underlying mechanisms for the observed differential $CD8^+$ T-cell infiltrate, TLS densities, and PD-L1 expression between responders and nonresponders, we performed targeted gene expression analysis by employing a commercially available targeted NGS assay (OIRRA) designed for the quantification of immune cell and inflammatory transcripts in FFPE samples. No significant differences nor strong tendencies in gene expression could be detected between responders and nonresponders in our cohort. Likewise, no correlations between gene expression profiles and the observed genetic alterations were found in opposite to recent reports,[7,8] even when focusing on known pathways like activation of the CCL5-CCR5 pathway in *BAP1* mutated ccRCC[41] or decreased STAT1 phosphorylation/decreased expression of interferon gamma target genes in *PBRM1* mutated ccRCC.[27] Still, potential differences within the tumor microenvironment cannot be excluded, because we used FFPE and not fresh frozen tissue for improved RNA quality and used a targeted RNAseq assay comprising 398 immune response related genes. Additional TCR sequencing suggested increased clonal T cells in responders. However, these results may correspond to pseudoclonality in view the few tumor-infiltrating T cells in responders, and must therefore be interpreted with caution.[42]

This focused study of ccRCC responder versus nonresponder samples has inherent shortcomings related to the number of samples, treatment heterogeneity, and limited documentation of the established RECIST criteria. However, we chose to focus on samples that represent the typically available tissue within pathology departments to probe which biomarkers may become feasible in clinical routine. Unique features demanding additional tissue requirements like slow-/or snap-frozen tumor and/or healthy control tissue will remain difficult to employ and may not prevail in the diagnostic routine. We achieved an in-depth analysis of RCC cases stratified by immunotherapy response through the combination of comprehensive molecular studies with spatially resolved tissue microenvironment analysis. Our results on conceptually novel biomarkers like tumor-infiltrating $CD8^+$ T cells[43] or TLS[9] and established biomarkers in immune oncology like PD-L1 expression are unexpected, remain unexplained and emphasize the need for further investigation in a larger cohort overcoming the limitations of our small sample size. Whether the combination of additional information such as blood parameters or a transcriptome-based molecular stratification of the samples[7] would provide a clear distinction remains to be determined, but certainly will not be feasible in the daily clinicopathologic routine.

ACKNOWLEDGMENTS

The authors thank Susanne Dettwiler and Fabiola Prutek from the Department of Pathology and Molecular Pathology, University Hospital Zurich for outstanding tissue management and technical assistance.

Conflicts of Interest/Financial Disclosures

Supported by the Promedica Foundation F-87701-41-01 (V.H.K.).

V.H.K. has served as an invited speaker on behalf of Indica Labs. The remaining authors have declared that there are no financial conflicts of interest with regard to this work.

REFERENCES

1. McDermott DF, Sosman JA, Sznol M, et al. Atezolizumab, an anti-programmed death-ligand 1 antibody, in metastatic renal cell carcinoma: long-term safety, clinical activity, and immune correlates from a phase Ia study. *J Clin Oncol*. 2016;34:833–842.
2. Motzer RJ, Penkov K, Haanen J, et al. Avelumab plus axitinib versus sunitinib for advanced renal-cell carcinoma. *N Engl J Med*. 2019;380:1103–1115.
3. Hasanov E, Gao J, Tannir NM. The immunotherapy revolution in kidney cancer treatment: scientific rationale and first-generation results. *Cancer J*. 2020;26:419–431.

4. Albiges L, Powles T, Staehler M, et al. Updated European Association of Urology Guidelines on Renal Cell Carcinoma: immune checkpoint inhibition is the new backbone in first-line treatment of metastatic clear-cell renal cell carcinoma. *Eur Urol*. 2019;76:151–156.
5. Binnewies M, Roberts EW, Kersten K, et al. Understanding the tumor immune microenvironment (TIME) for effective therapy. *Nat Med*. 2018;24:541–550.
6. Bi K, He MX, Bakouny Z, et al. Tumor and immune reprogramming during immunotherapy in advanced renal cell carcinoma. *Cancer Cell*. 2021;39:649–661e5.
7. Motzer RJ, Banchereau R, Hamidi H, et al. Molecular subsets in renal cancer determine outcome to checkpoint and angiogenesis blockade. *Cancer Cell*. 2020;38:803–817e4.
8. Brugarolas J, Rajaram S, Christie A, et al. The evolution of angiogenic and inflamed tumors: the renal cancer paradigm. *Cancer Cell*. 2020;38:771–773.
9. Helmink BA, Reddy SM, Gao J, et al. B cells and tertiary lymphoid structures promote immunotherapy response. *Nature*. 2020;577:549–555.
10. Turajlic S, Litchfield K, Xu H, et al. Insertion-and-deletion-derived tumour-specific neoantigens and the immunogenic phenotype: a pan-cancer analysis. *Lancet Oncol*. 2017;18:1009–1021.
11. Hansen UK, Ramskov S, Bjerregaard AM, et al. Tumor-infiltrating T cells from clear cell renal cell carcinoma patients recognize neoepitopes derived from point and frameshift mutations. *Front Immunol*. 2020;11:373.
12. Hegde PS, Karanikas V, Evers S. The where, the when, and the how of immune monitoring for cancer immunotherapies in the era of checkpoint inhibition. *Clin Cancer Res*. 2016;22:1865–1874.
13. Noman MZ, Desantis G, Janji B, et al. PD-L1 is a novel direct target of HIF-1alpha, and its blockade under hypoxia enhanced MDSC-mediated T cell activation. *J Exp Med*. 2014;211:781–790.
14. Ruf M, Moch H, Schraml P. PD-L1 expression is regulated by hypoxia inducible factor in clear cell renal cell carcinoma. *Int J Cancer*. 2016;139:396–403.
15. Nakano O, Sato M, Naito Y, et al. Proliferative activity of intratumoral CD8(+) T-lymphocytes as a prognostic factor in human renal cell carcinoma: clinicopathologic demonstration of antitumor immunity. *Cancer Res*. 2001;61:5132–5136.
16. Granier C, Dariane C, Combe P, et al. Tim-3 expression on tumor-infiltrating PD-1(+)CD8(+) T cells correlates with poor clinical outcome in renal cell carcinoma. *Cancer Res*. 2017;77:1075–1082.
17. Nienhold R, Ciani Y, Koelzer VH, et al. Two distinct immunopathological profiles in autopsy lungs of COVID-19. *Nat Commun*. 2020;11:5086.
18. Aryee MJ, Jaffe AE, Corrada-Bravo H, et al. Minfi: a flexible and comprehensive Bioconductor package for the analysis of Infinium DNA methylation microarrays. *Bioinformatics*. 2014;30:1363–1369.
19. Becht E, McInnes L, Healy J, et al. Dimensionality reduction for visualizing single-cell data using umap. *Nat Biotechnol*. 2019;37:38.
20. Haefliger S, Tzankov A, Frank S, et al. NUT midline carcinomas and their differentials by a single molecular profiling method: a new promising diagnostic strategy illustrated by a case report. *Virchows Arch*. 2021;478:1007–1012.
21. Lawrence M, Huber W, Pages H, et al. Software for computing and annotating genomic ranges. *PLoS Comput Biol*. 2013;9:e1003118.
22. Capper D, Jones DTW, Sill M, et al. DNA methylation-based classification of central nervous system tumours. *Nature*. 2018;555:469–474.
23. Skidmore ZL, Wagner AH, Lesurf R, et al. GenVisR: Genomic Visualizations in R. *Bioinformatics*. 2016;32:3012–3014.
24. Amgad M, Stovgaard ES, Balslev E, et al. Report on computational assessment of tumor infiltrating lymphocytes from the International Immuno-Oncology Biomarker Working Group. *NPJ Breast Cancer*. 2020;6:16.
25. Zhu J, Armstrong AJ, Friedlander TW, et al. Biomarkers of immunotherapy in urothelial and renal cell carcinoma: PD-L1, tumor mutational burden, and beyond. *J Immunother Cancer*. 2018;6:4.
26. Jacquelot N, Tellier J, Nutt SI, et al. Tertiary lymphoid structures and B lymphocytes in cancer prognosis and response to immunotherapies. *Oncoimmunology*. 2021;10:1900508.
27. Liu XD, Kong W, Peterson CB, et al. PBRM1 loss defines a nonimmunogenic tumor phenotype associated with checkpoint inhibitor resistance in renal carcinoma. *Nat Commun*. 2020;11:2135.
28. Miao D, Margolis CA, Gao W, et al. Genomic correlates of response to immune checkpoint therapies in clear cell renal cell carcinoma. *Science*. 2018;359:801–806.
29. Ricketts CJ, De Cubas AA, Fan H, et al. The cancer genome atlas comprehensive molecular characterization of renal cell carcinoma. *Cell Rep*. 2018;23:313–326e5.
30. Moch H, Cubilla AL, Humphrey PA, et al. The 2016 WHO Classification of Tumours of the Urinary System and Male Genital Organs—Part A: renal, penile, and testicular tumours. *Eur Urol*. 2016;70:93–105.
31. Mamlouk S, Childs LH, Aust D, et al. DNA copy number changes define spatial patterns of heterogeneity in colorectal cancer. *Nat Commun*. 2017;8:14093.
32. Yoshimoto T, Matsuura K, Karnan S, et al. High-resolution analysis of DNA copy number alterations and gene expression in renal clear cell carcinoma. *J Pathol*. 2007;213:392–401.
33. Beroukhim R, Brunet JP, Di Napoli A, et al. Patterns of gene expression and copy-number alterations in von-hippel lindau disease-associated and sporadic clear cell carcinoma of the kidney. *Cancer Res*. 2009;69:4674–4681.
34. Nouhaud FX, Blanchard F, Sesboue R, et al. Clinical relevance of gene copy number variation in metastatic clear cell renal cell carcinoma. *Clin Genitourin Cancer*. 2018;16:e795–e805.
35. Salgado R, Denkert C, Demaria S, et al. The evaluation of tumor-infiltrating lymphocytes (TILs) in breast cancer: recommendations by an International TILs Working Group 2014. *Ann Oncol*. 2015;26:259–271.
36. Waldman AD, Fritz JM, Lenardo MJ. A guide to cancer immunotherapy: from T cell basic science to clinical practice. *Nat Rev Immunol*. 2020;20:651–668.
37. Giraldo NA, Becht E, Vano Y, et al. Tumor-infiltrating and peripheral blood T-cell immunophenotypes predict early relapse in localized clear cell renal cell carcinoma. *Clin Cancer Res*. 2017;23:4416–4428.
38. Stenzel PJ, Schindeldecker M, Tagscherer KE, et al. Prognostic and predictive value of tumor-infiltrating leukocytes and of immune checkpoint molecules PD1 and PDL1 in clear cell renal cell carcinoma. *Transl Oncol*. 2020;13:336–345.
39. Davis D, Tretiakova MS, Kizzar C, et al. Abundant CD8+ tumor infiltrating lymphocytes and beta-2-microglobulin are associated with better outcome and response to interleukin-2 therapy in advanced stage clear cell renal cell carcinoma. *Ann Diagn Pathol*. 2020;47:151537.
40. Callea M, Albiges L, Gupta M, et al. Differential expression of PD-L1 between primary and metastatic sites in clear-cell renal cell carcinoma. *Cancer Immunol Res*. 2015;3:1158–1164.
41. Zhou Q, Qi Y, Wang Z, et al. CCR5 blockade inflames antitumor immunity in BAP1-mutant clear cell renal cell carcinoma. *J Immunother Cancer*. 2020;8:1.
42. Groenen PJ, Langerak AW, van Dongen JJ, et al. Pitfalls in TCR gene clonality testing: teaching cases. *J Hematop*. 2008;1:97–109.
43. Koelzer VH, Sirinukunwattana K, Rittscher J, et al. Precision immunoprofiling by image analysis and artificial intelligence. *Virchows Arch*. 2019;474:511–522.

